# Hydrodynamic Modelling at Aird Point (Etive 4) and Sailean Ruadh (Etive 6) sites

## CAR/L/1018068 (Aird Point, Etive 4)
## CAR/L/1042067 (Sailean Ruadh, Etive 6)
## March 2025


Mowi Scotland

OFFICE
Mowi, Farms Office, Glen Nevis Business Park
PH33 6RX Fort William

POSTAL
Mowi, Farms Office, Glen Nevis Business Park
PH33 6RX Fort William

PHONE

FAX
-

MAIL
environment@mowi.com

WEB
http://mowiscotland.co.uk

# CONTENTS

# LIST OF FIGURES

# LIST OF TABLES

## QUALITY ASSURANCE

Mowi Scotland Ltd is ISO9001 and ISO14001 accredited and all project management follows policies designed to ensure that the collection, collation and reporting of information produced in the course of our operations is done to a consistently high standard meeting the requirements of the end user.

# 1. Introduction

This report has been prepared by Mowi Scotland Ltd. to meet the requirements of the Scottish Environment Protection Agency (SEPA) for an application to use topical sealice veterinary medicines at the **Aird Point (Etive 4)** and **Sailean Ruadh (Etive 6)** marine salmon farms in **Loch Etive** (Figure 1). The application uses coupled hydrodynamic and particle tracking modelling to describe the dispersion of bath treatments in order to determine EQS-compliant quantities for the current site biomass and equipment. This report describes the configuration, calibration and validation of the hydrodynamic model used in the application. The dispersion modelling for each site is described in separate reports (Mowi 2025a, b).

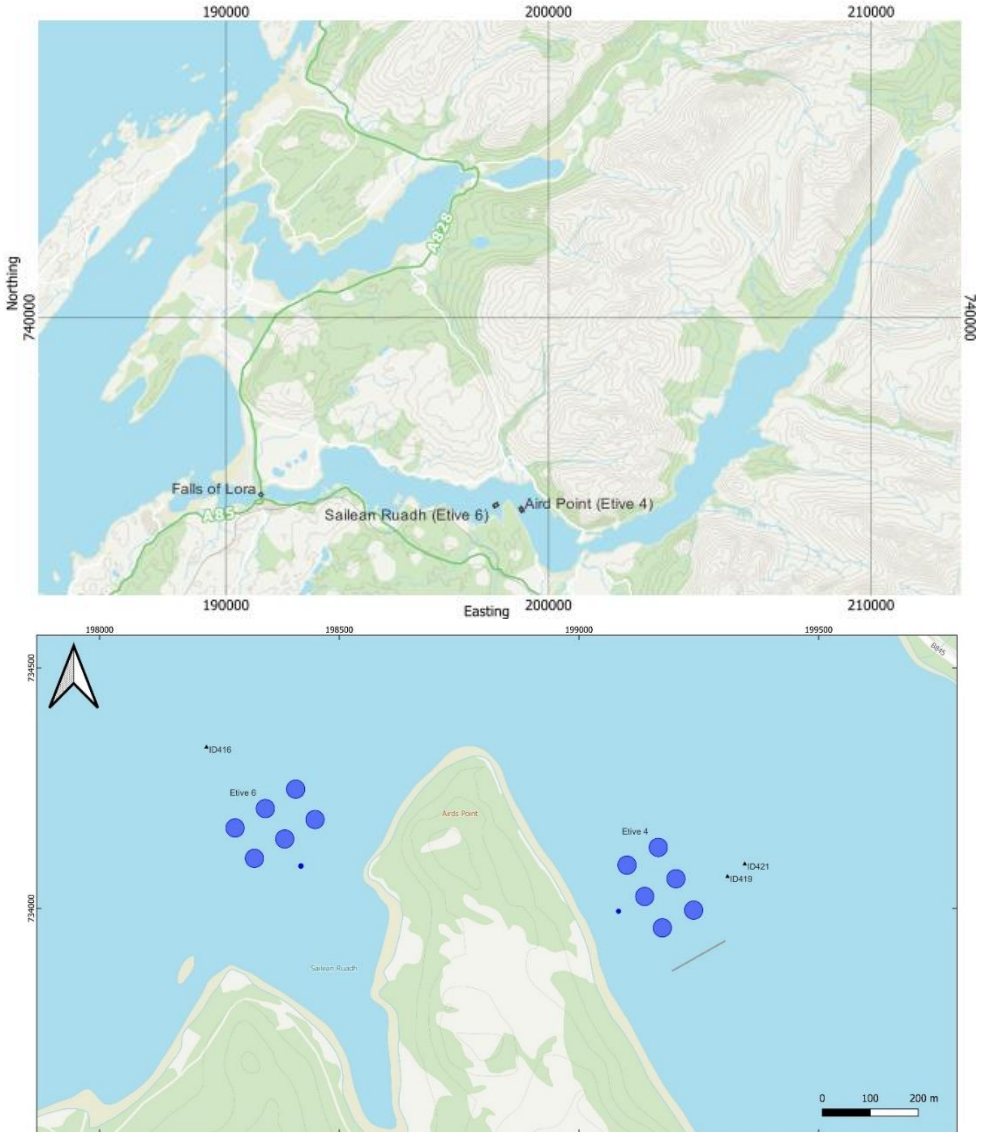


*Figure 1. Locations of the Aird Point (Etive 4) and Sailean Ruadh (Etive 6) sites in Loch Etive (top) and the layout of the 120m pens (●) bottom. The locations of the current meter (ADCP) deployments are shown.*

### 1.1 Site Description

Loch Etive is an extremely challenging environment for hydrodynamic models to simulate. The shallow entrance sill at the Falls of Lora, Connell, has a strong tidal choking (Stigebrandt, 1980) effect, leading to a 50% reduction in the tidal range within Loch Etive relative to the range in the adjacent coastal waters (Edwards and Edelsten, 1977). The very strong frictional forces at these locations tend to destabilise coastal hydrodynamic models, possibly because non-hydrostatic effects are so strong. As a result, the frictional effects must necessarily be diminished within the model and the simulated tidal choking not as strongly reproduced as in reality. For example, we need to impose a minimum water depth of 5 m within the model domain, which is deeper than the actual depths in the Falls of Lora, in order to keep the model stable. While this leads to relatively poor simulation of the sea surface height (SSH) within the loch, tidal choking effects on current speed and direction are very localized at the sill, and the hydrodynamic models are still able to simulate water velocity reasonably well within and outside the loch (Mowi, 2024).

For example, the Wider Loch Linnhe System (WLLS) model does not fully reproduce the tidal choking effect on the SSH in Loch Etive, with the simulated tidal range noticeably greater than the observed range. However, some choking does occur, with the tidal amplitude in the loch reduced relative to that outside the loch. Importantly, the model still reproduces the magnitude of the current speed and direction within the loch reasonably well, although there is some offset due to an over-estimated density-driven circulation.

Medicine dispersion is predominantly driven by current speed and direction, and is relatively uninfluenced by sea surface height. Therefore, for the purposes of this study, we will focus the model calibration on velocity and not attempt to force the model to reproduce the full tidal choking effect on sea surface height.

## 2. Model Description

The hydrodynamic model used was FVCOM (Finite Volume Community Ocean Model), a prognostic, unstructured-grid, finite-volume, free-surface, 3-D primitive equation coastal ocean circulation model developed by the University of Massachusetts School of Marine Science and the Woods Hole Oceanographic Institute (Chen et al., 2003). The model consists of equations describing the evolution and conservation of momentum, temperature, salinity and turbulence parameters, the latter using a turbulence closure submodel. The horizontal grid is comprised of unstructured triangular cells and the irregular bottom is presented using generalized terrain-following coordinates. The General Ocean Turbulent Model (GOTM) developed by Burchard's research group in Germany (Burchard, 2002) has been added to FVCOM to provide optional vertical turbulent closure schemes. Horizontal viscosity and diffusivity was calculated using the Smagorinsky algorithm, with a coefficient value $c_s$. FVCOM is solved numerically by a second-order accurate discrete flux calculation in the integral form of the governing equations over an unstructured triangular grid. This approach combines the best features of finite-element methods (grid flexibility) and finite-difference methods (numerical efficiency and code simplicity) and provides a much better numerical representation of both local and global momentum, mass, salt, heat, and tracer conservation. The ability of FVCOM to accurately solve scalar conservation equations in addition to the topological flexibility provided by unstructured meshes and the simplicity of the coding structure has make FVCOM ideally suited for many coastal and interdisciplinary scientific applications, such as typically found in

Scotland. The mesh flexibility allows greater spatial resolution in near-shore areas without excessive computational demand.

The model is forced by a tidal condition along the open boundary, and by frictional stresses at the surface and seabed. At the seabed, the frictional stress, $\boldsymbol{\tau}_b$, is calculated using a quadratic equation where:

$$\tau_b = \rho C_D \boldsymbol{U}|\boldsymbol{U}| \quad (1)$$

where ρ = 1025 kg m$^{-3}$ is the water density, **U** is the velocity in the layer closest to the seabed. The drag coefficient, $C_D$, is calculated from the bed roughness lengthscale, $z_0$, using:

$$C_D = \left(\frac{\kappa}{\ln\left(\frac{z_b+z_0}{z_0}\right)}\right)^2 \quad (2)$$

where κ=0.4 is von Karman's constant, and $z_b$ is the height above the bed of the lowest velocity point. The value of $z_0$ was varied during calibration to provide the best fit to observations of sea level and velocity.

Wind forcing is applied as a surface stress calculated from hourly wind speed and direction. Wind stress is calculated from the wind velocity by a standard quadratic relation:

$$\tau_x = \rho_a C_W u W \quad (3a)$$
$$\tau_y = \rho_a C_W v W \quad (3b)$$

where (u,v) are the East and North components of wind velocity respectively, W is the wind speed ($W = [u^2+v^2]^{½}$), $\rho_a$ is the density of air, and the surface drag coefficient $C_W$ is calculated following Large and Pond (1981).

## 3. Configuration and Boundary Forcing for Loch Etive

The Etive 4 and 6 sites are situated in Loch Etive in Argyll north of Oban (Figure 1). The unstructured mesh used in the modelling (Figure 2) was adapted from a customised Loch Linnhe mesh subdomain of the Wider Loch Linnhe System (WLLS), with open water boundaries in the Firth of Lorn and the Sound of Mull. Model resolution was enhanced in the Loch Etive region particularly around the Mowi sites at Aird Point and Sailean Ruadh (Figure 3).

The spatial resolution of the model varied from 29 m in some inshore waters and round the farm pens to 180 m along the open boundary. The model consisted of 33,393 nodes and 59,893 triangular elements.

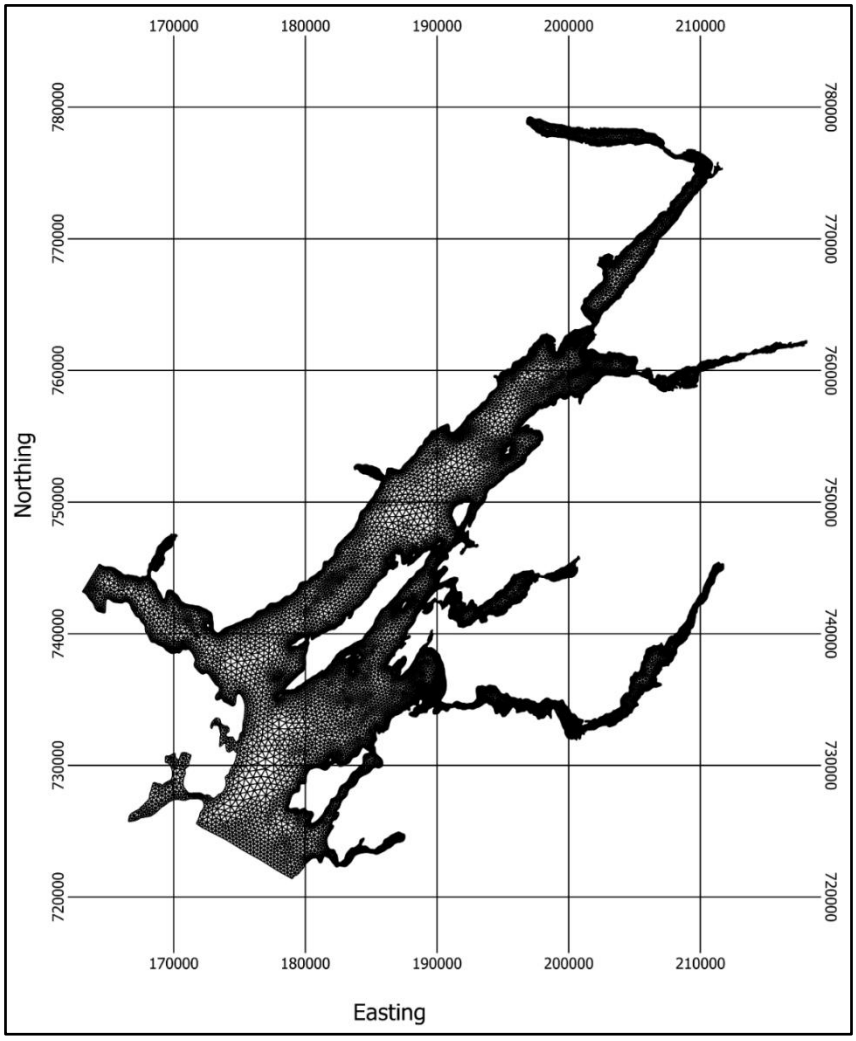


*Figure 2. The mesh and domain of the Loch Linnhe and Loch Etive model.*

Model bathymetry (Figure 4) was taken from the WLLS model with the addition of bathymetry data collected from a multibeam depth survey available through the Admiralty Seabed Mapping Service (https://www.admiralty.co.uk/access-data).

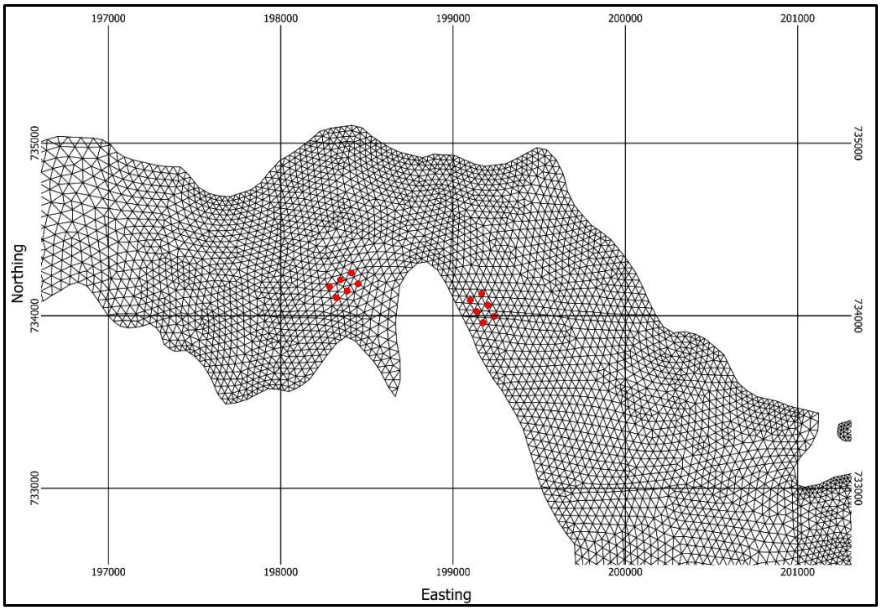


Figure 3. *The unstructured mesh around the Aird Point (Etive 4) and Sailean Ruadh (Etive 6) sites in the modified model grid, with the pen locations indicated (●).*

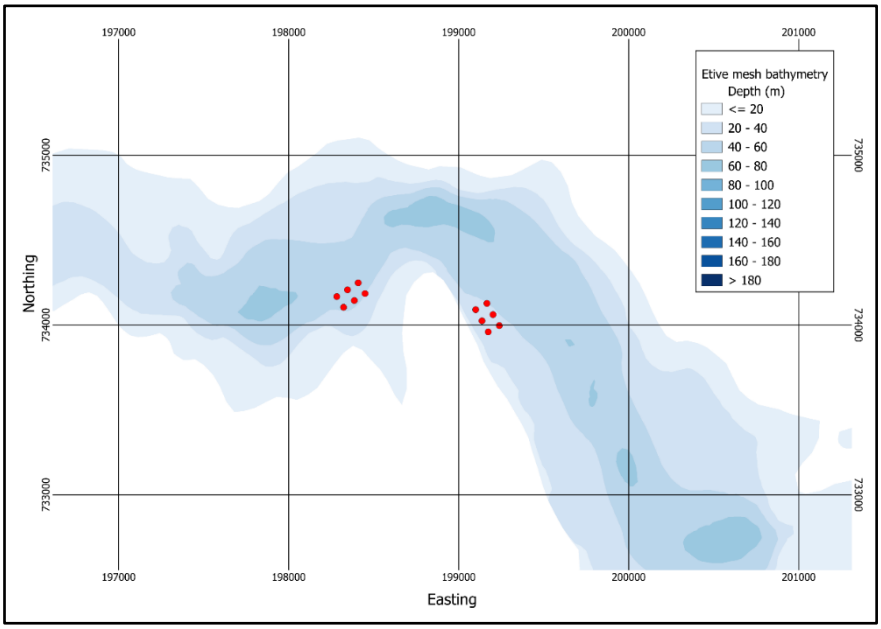


*Figure 4. Model water depths (m) in the area around the Aird Point (Etive 4) and Sailean Ruadh (Etive 6) salmon farm sites. The pen locations are indicated (●).*

The model was forced along its open boundary by time series of sea surface height (SSH) at each boundary node for the relevant simulation periods; FVCOM appears to perform better when boundary forcing is applied as a time series rather than when tidal constituents are used. The SSH time series were generated using the RiCOM hydrodynamic model (Walters and Casulli, 1998; Gillibrand et al., 2016b) on the Scottish Shelf Model WLLS grid (Marine Scotland,

2016), which was, in turn, forced by eight tidal constituents ($O_1$, $K_1$, $Q_1$, $P_1$, $M_2$, $S_2$, $N_2$, $K_2$) taken from the full Scottish Shelf model (SSM).

Spatially- and temporally-varying wind speed and direction data were taken for the required simulation periods from the Weather Research & Forecasting (WRF) model, developed as part of the WestCOMS modelling suite (Aleynik et al., 2016).

Stratification was expected to be significant in this area and the model was run in 3D baroclinic mode. Fourteen layers in the vertical (fifteen sigma levels) were used in the simulations, with layers concentrated near the surface and seabed. The sigma levels used were:

σ = [0.00 -0.01 -0.04 -0.09 -0.16 -0.25 -0.37 -0.50 -0.63 -0.75 -0.84 -0.91 -0.96 -0.99 -1.00]

Ten rivers were input into the model domain, including the rivers Etive and Awe into Loch Etive. River flows were catchment-weighted based on data for the Lochy and Orchy rivers from the National River Flow Archive (NRFA, https://nrfa.ceh.ac.uk/).

# 4. Model Calibration and Validation

The local area model was calibrated and validated against current data and seabed pressure data, measured near the two sites using Acoustic Doppler Current Profilers (ADCP, Figure 1). Data were available from:

(i) Calibration: 20th June – 7th August 2023 (ID419)
(ii) Validation: 27th April – 26th July 2023 (ID416)
(iii) Validation: 7th August – 12th October 2023 (ID421)

In total, the data extend over 156 days. Calibration was performed in a standard fashion, with bed friction roughness, $C_D$, and the Smagorinsky viscosity coefficient, $c_s$, being adjusted to obtain the best fit against the sea surface height and current data. Once the best comparison with the calibration data was achieved, the parameter set was tested without further adjustment against the validation dataset.

## 4.1 Calibration: 20th June – 7th August 2023 (ID419, Etive 4)

The calibration used observed depth and current velocity from an ADCP location at Aird Point (Etive 4) to compare with modelled sea surface height (SSH) and velocity (ADCP deployment ID419). Simulations were performed with a range of values of both parameters. After a number of simulations, a final parameter set was selected (Table 1).

The results of the calibration exercise for ID419 are presented in Figure 5 – Figure 8 and Table 2. At the ADCP location, the modelled sea surface height displayed a greater range than observed (Figure 5), due to the challenges of modelling the tidal choking over the sill at the Falls of Lora as described above. The model skill was 0.94 and the mean absolute error (MAE) and root-mean-square error (RMSE) values were 0.23 m and 0.28 respectively. Despite this relatively poor agreement in sea surface height prediction, the modelled velocity compared acceptably well with the observed data.

*Table 1. Parameter values chosen for the FVCOM model during the calibration simulations.*

| Parameter Description | Value |
|---|---|
| Bed roughness lengthscale, $z_0$ (m) | 0.01 |
| Smagorinsky coefficient, $c_s$ ($m^2$ $s^{-1}$) | 0.2 |
| Number of vertical layers | 14 |
| Barotropic time step (s) | 0.5 |
| Baroclinic time step (s) | 2.0 |

For the East and North components of near-surface (6.4 m) velocity (Figure 6), the model skill scores were 0.69 and 0.73 respectively, with RMSE values of 0.07 m $s^{-1}$ and 0.12 m $s^{-1}$ for the two components of velocity respectively (Table 2). At the deeper depth of 16.4 m, the skill scores were similar, at 0.75 and 0.71 respectively. The MAE and RMSE values were less than those at the shallower depth, in the range 0.03 m $s^{-1}$ – 0.06 m $s^{-1}$. At the deeper depth (43.4 m), model performance was slightly reduced (Table 2), but is less relevant to medicine dispersion simulations.

The histograms and scatter plots (Figure 7 and Figure 8) demonstrate that the modelled current had broadly the same magnitude and direction characteristics as the observed data. For further context, the observed and modelled profiles of mean velocity and mean speed are presented in *Figure **9.** Profiles of observed and modelled mean velocity (East, North) and mean speed, calculated over the full simulation from 20th June – 7th August 2023.*Figure 9. The profiles illustrate the rapid change in current speed in the upper water column; any inaccuracy in the modelled velocity profile can lead to large apparent errors in the model-data comparison at specific depths. Overall, the model performs reasonably well at reproducing the observed profiles. Similarly, the results from a tidal analysis of the modelled and observed velocity using T-TIDE (Pawlowicz et al., 2002) demonstrate that the model reproduces the main features of the $M_2$ and $S_2$ tidal constituent profiles (Figure 10), but illustrates the potential for apparent errors in the model-data comparison due to the rapid change in $M_2$ velocity amplitude particularly in the top 15 m of the water column.

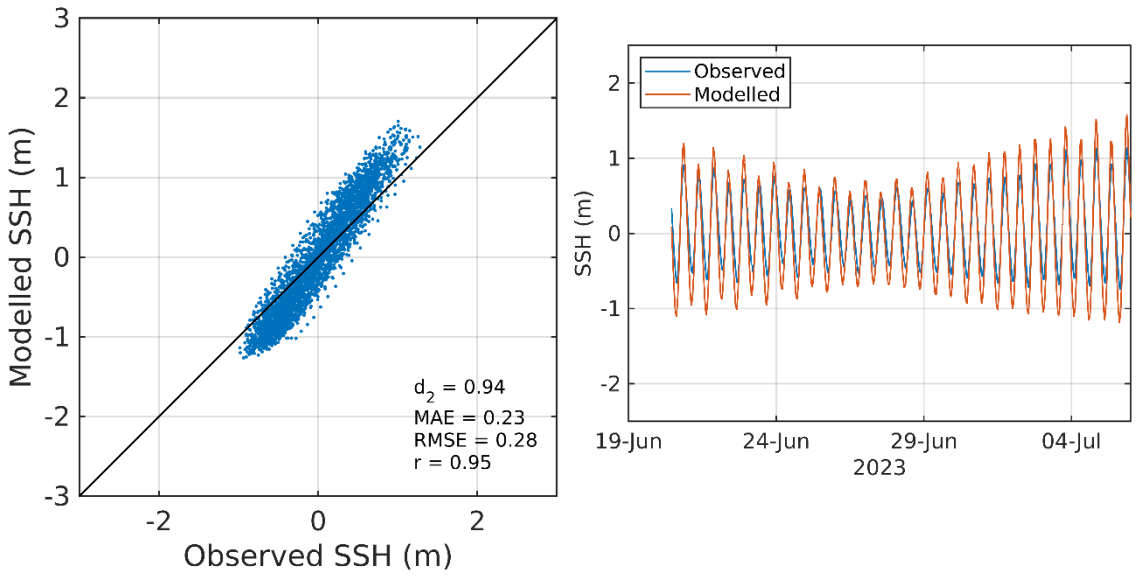


*Figure 5. Comparison between observed and modelled sea surface height from ID419 using model parameter values from Table 1. Both the full record (left) and a subset of 15 days (right) are shown. In the latter, the observed data are in blue, model results in red.*

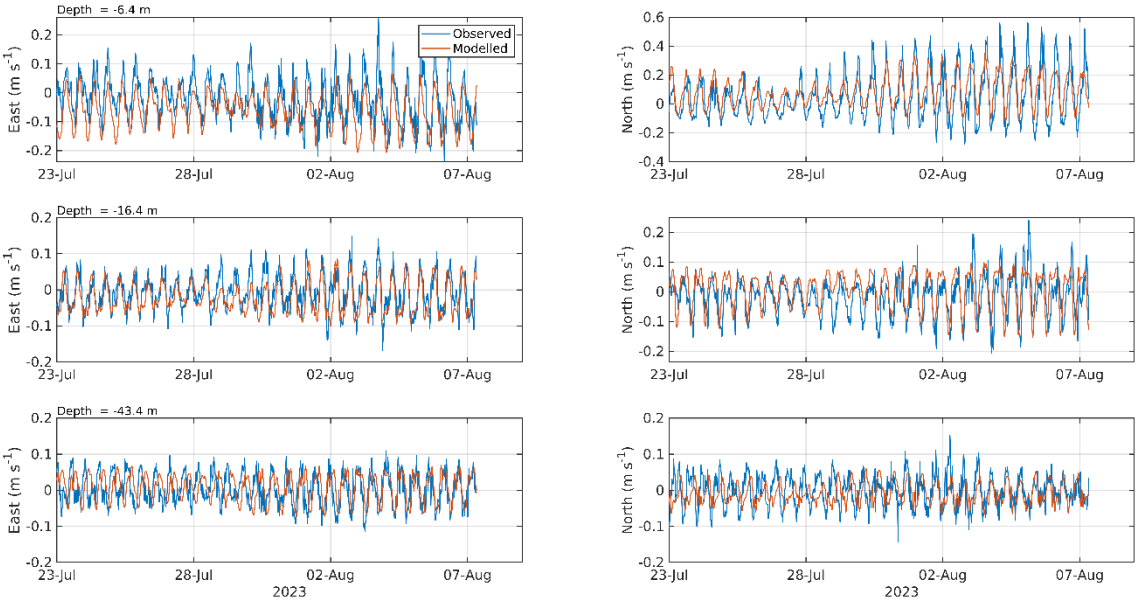


*Figure 6. Comparison between observed and modelled East (left) and North (right) components of velocity at the ADCP location for 15 days in July – August 2023 (ID419) at three depths: 6.4 m (top), 16.4 m (middle) and 43.4 m (bottom). Observed data are in blue, model results in red.*

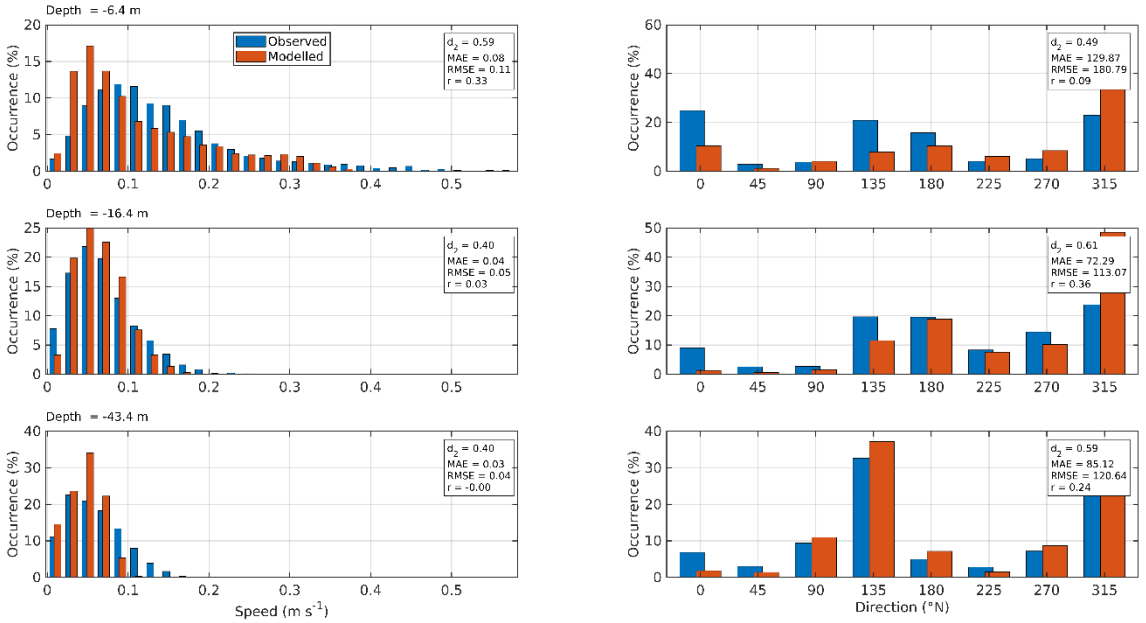


*Figure 7. Histograms of observed and modelled speed (left) and direction (right) at the ADCP location for July – August 2023 (ID419) at three depths: 6.4 m (top), 16.4 m (middle) and 43.4 m (bottom). Observed data are in blue, model results in red.*

*Table 2. Model performance statistics for sea surface height (SSH) and East and North velocity at the ADCP location from 20 June – 07 August 2023 (ID419) at three depths (6.4 m, 16.4 m and 43.4 m).*

| | | Skill, $d_2$ | MAE | RMSE |
|---|---|---|---|---|
| Sea Surface Height (SSH, m) | | 0.94 | 0.23 | 0.28 |
| 6.4 m | East Velocity (m $s^{-1}$) | 0.69 | 0.06 | 0.07 |
| | North Velocity (m $s^{-1}$) | 0.73 | 0.10 | 0.12 |
| 16.4 m | East Velocity (m $s^{-1}$) | 0.75 | 0.03 | 0.04 |
| | North Velocity (m $s^{-1}$) | 0.71 | 0.05 | 0.06 |
| 43.4 m | East Velocity (m $s^{-1}$) | 0.64 | 0.05 | 0.06 |
| | North Velocity (m $s^{-1}$) | 0.58 | 0.04 | 0.05 |

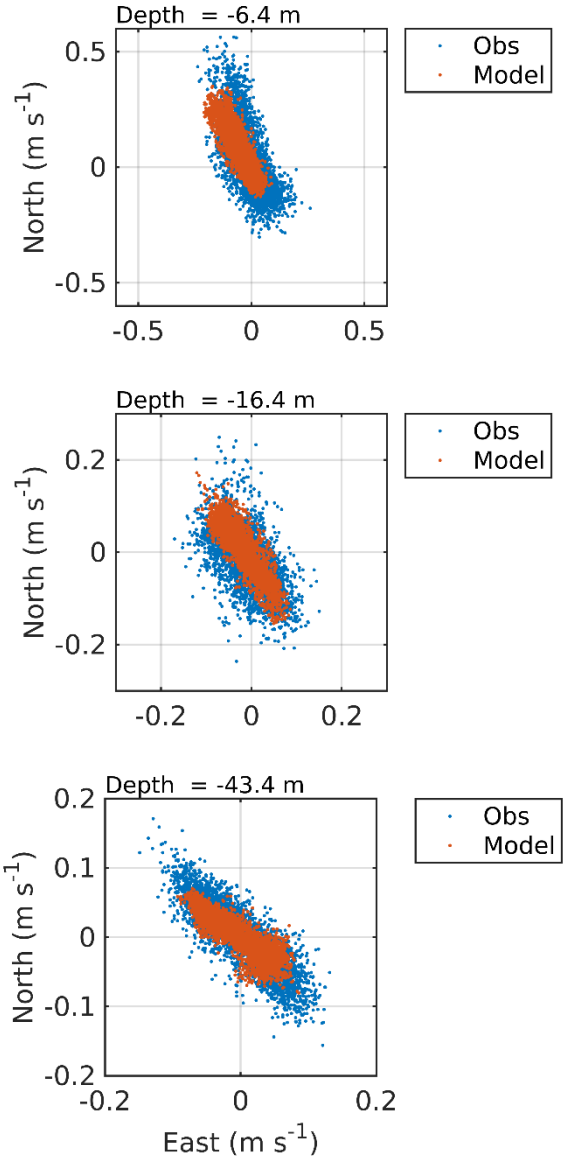


*Figure 8. Scatter plot of observed and modelled velocity at the ADCP location for June – August 2023 (ID419) at three depths: 6.4 m (top), 16.4 m (middle) and 43.4 m (bottom). Observed data are in blue, model results in red.*

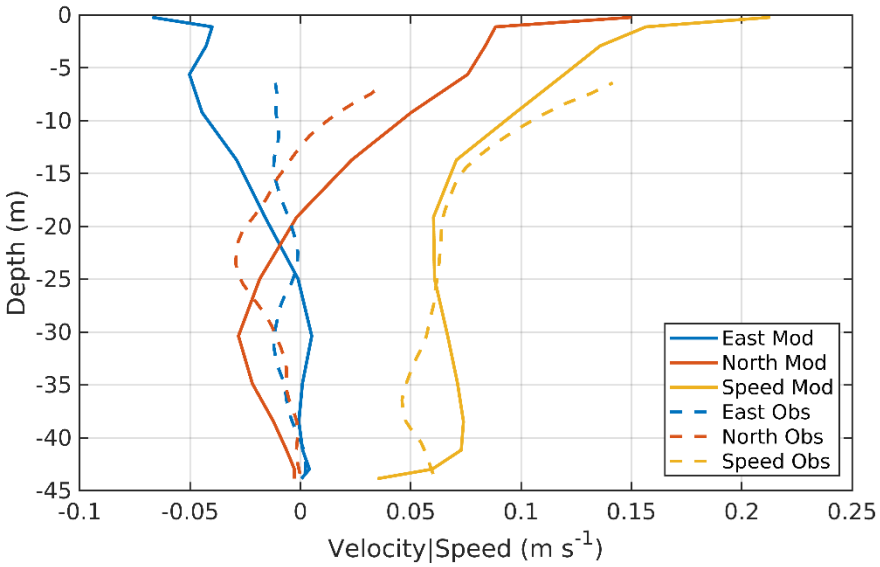


*Figure 9. Profiles of observed and modelled mean velocity (East, North) and mean speed, calculated over the full simulation from 20th June – 7th August 2023.*

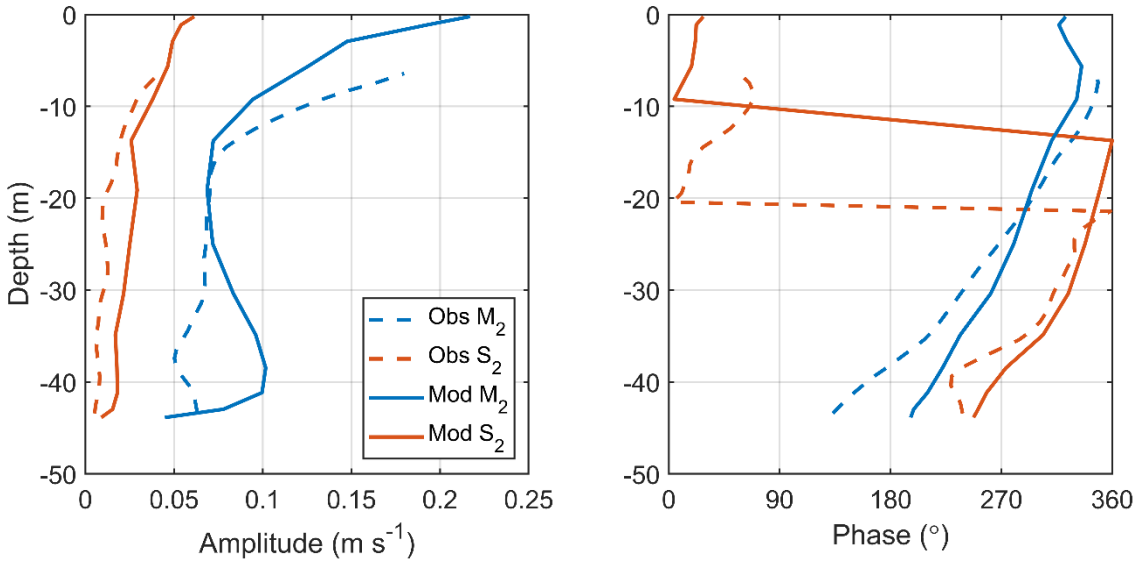


*Figure 10. Profiles of observed and modelled amplitude (left) and phase (right) of the $M_2$ and $S_2$ constituents of tidal velocity, calculated from the full simulation from 20th June – 7th August 2023.*

## 4.2 Validation: 27th April – 26th July 2023 (ID416, Etive 6)

As with the calibration simulation, the model did not fully reproduce the tidal choking across the Falls of Lora sill, and the tidal range inside Loch Etive was over-predicted (Figure 11), with a model skill of 0.93 and mean absolute error (MAE) and root-mean-square error (RMSE) values of 0.27 m and 0.31 respectively (Table 3).

For the East and North components of near-surface (6.5 m) velocity (Figure 12), model skill scores were 0.64 and 0.53 respectively, with RMSE values of 0.11 m $s^{-1}$ and 0.09 m $s^{-1}$ for the two components of velocity. The model performance metrics were brodly similar for the deeper depths (Table 3).

The histograms and scatter plots shown in Figure 14 and Figure 13 demonstrate that the modelled currents were broadly of the same speed and direction as the observed data. The profiles of observed and modelled velocity and speed (Figure 15) show that the model did not quite capture the current velocity profiles correctly, but that the mean current speed at the site was well simulated.

*Table 3. Model performance statistics for sea surface height (SSH), and East and North velocity at the ADCP location from April – July 2023 (ID416) at three depths, 6.5 m, 16.5 m and 48.5 m.*

| | | Skill, $d_2$ | MAE | RMSE |
|---|---|---|---|---|
| Sea Surface Height (SSH, m) | | 0.93 | 0.27 | 0.31 |
| 6.5 m | East Velocity (m $s^{-1}$) | 0.64 | 0.09 | 0.11 |
| | North Velocity (m $s^{-1}$) | 0.53 | 0.07 | 0.09 |
| 16.5 m | East Velocity (m $s^{-1}$) | 0.74 | 0.06 | 0.08 |
| | North Velocity (m $s^{-1}$) | 0.64 | 0.05 | 0.06 |
| 48.5 m | East Velocity (m $s^{-1}$) | 0.59 | 0.05 | 0.06 |
| | North Velocity (m $s^{-1}$) | 0.55 | 0.04 | 0.05 |

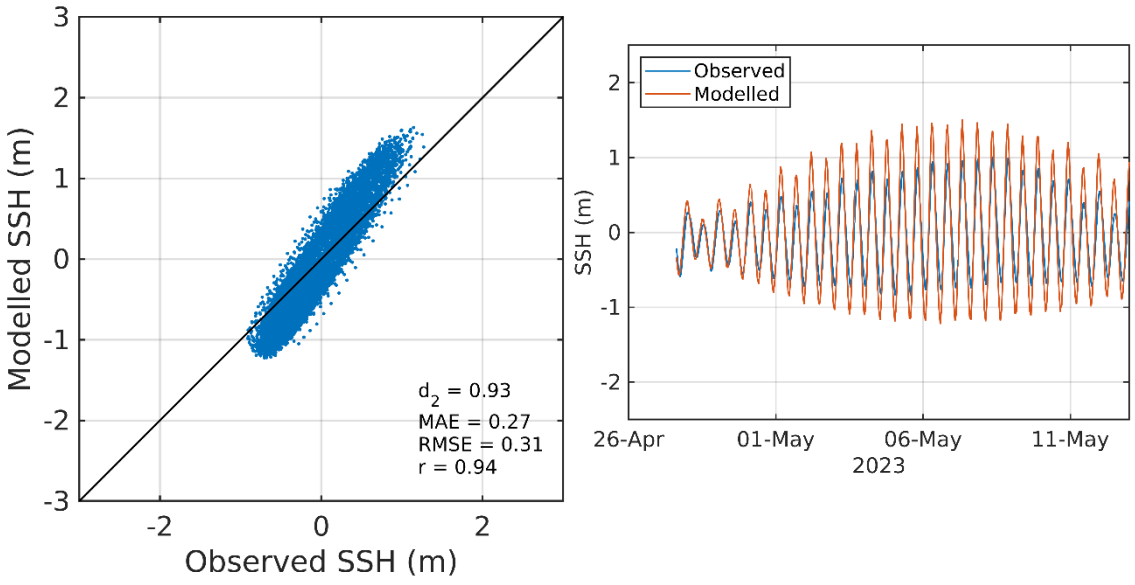


*Figure 11. Comparison between observed and modelled sea surface height from April – July 2023 (ADCP deployment ID416) using model parameter values from Table 1. Both the full record (left) and a subset of 15 days (right) are shown. Observed data are in blue, model results in red.*

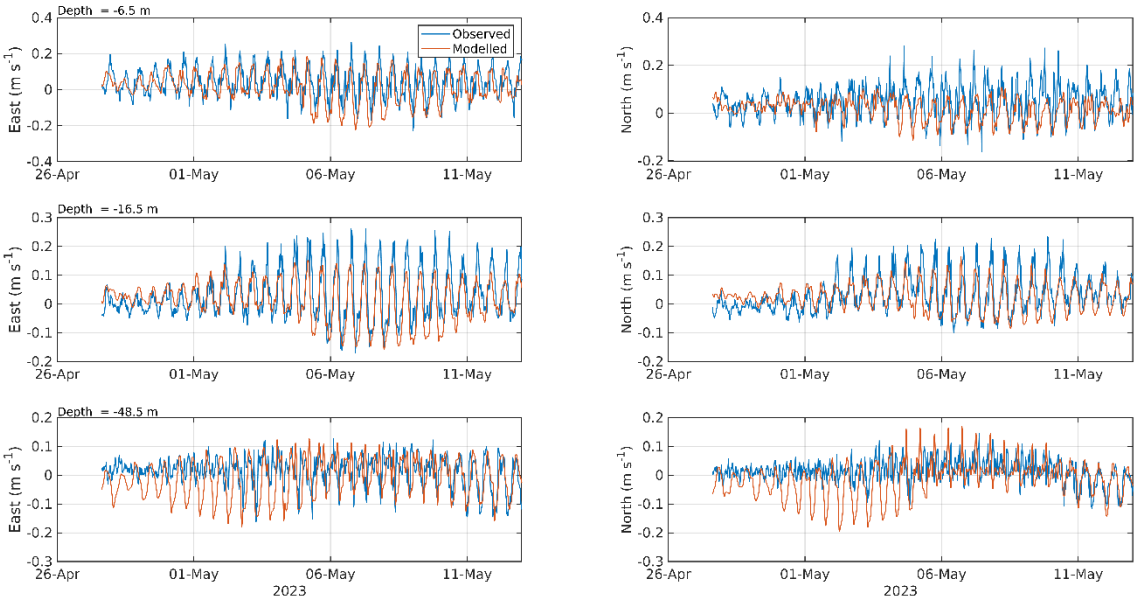


*Figure 12. Comparison between observed and modelled East (left) and North (right) components of velocity at the ADCP location for 15 days in April – May 2023 (ID416) at three depths, 6.5 m (top), 16.5 m (middle) and 48.5 m (bottom). Observed data are in blue, model results in red.*

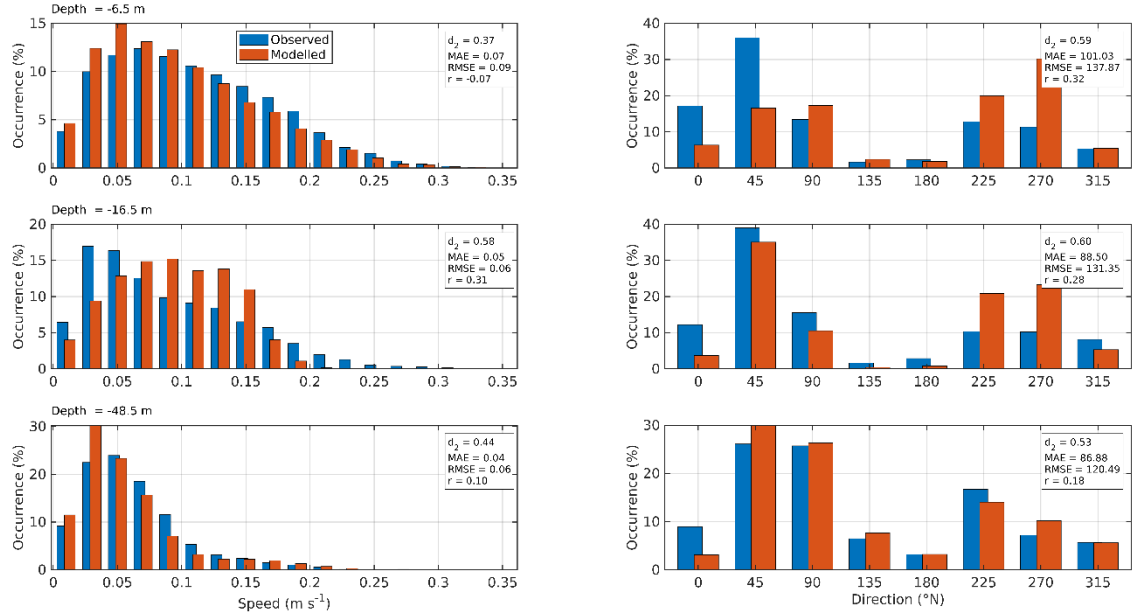


*Figure 13. Histograms of observed and modelled current speed (left) and direction (right) at the ADCP location from April – July 2023 (ID416) at three depths, 6.5 m (top), 16.5 m (middle) and 48.5 m (bottom). Observed data are in blue, model results in red.*

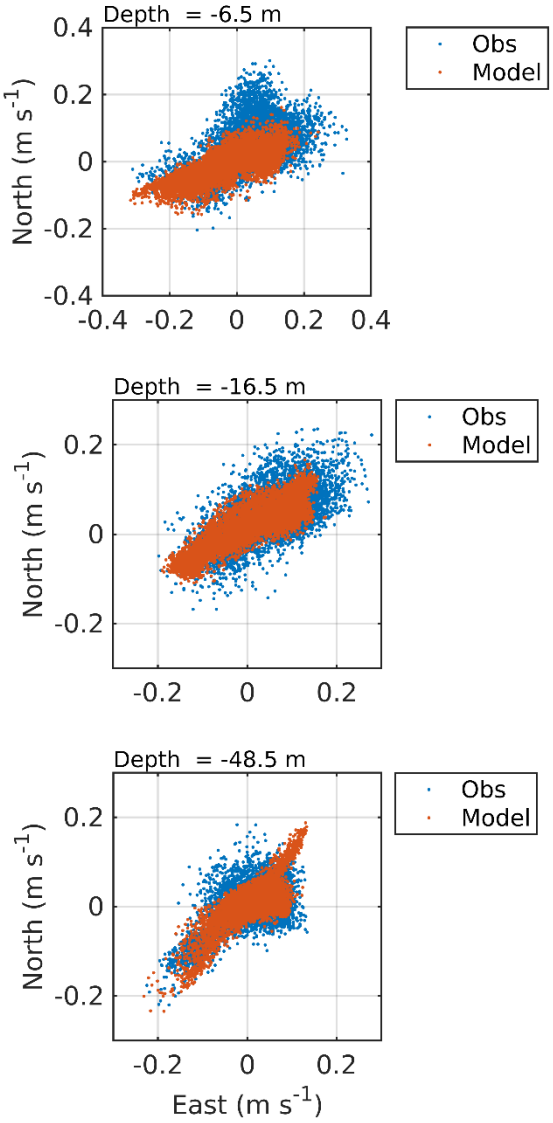


*Figure 14. Scatter plot of observed and modelled velocity at the ADCP location from April – July 2023 (ID416) at three depths, 6.5 m (top), 16.5 m (middle) and 48.5 m (bottom). Observed data are in blue, model results in red.*

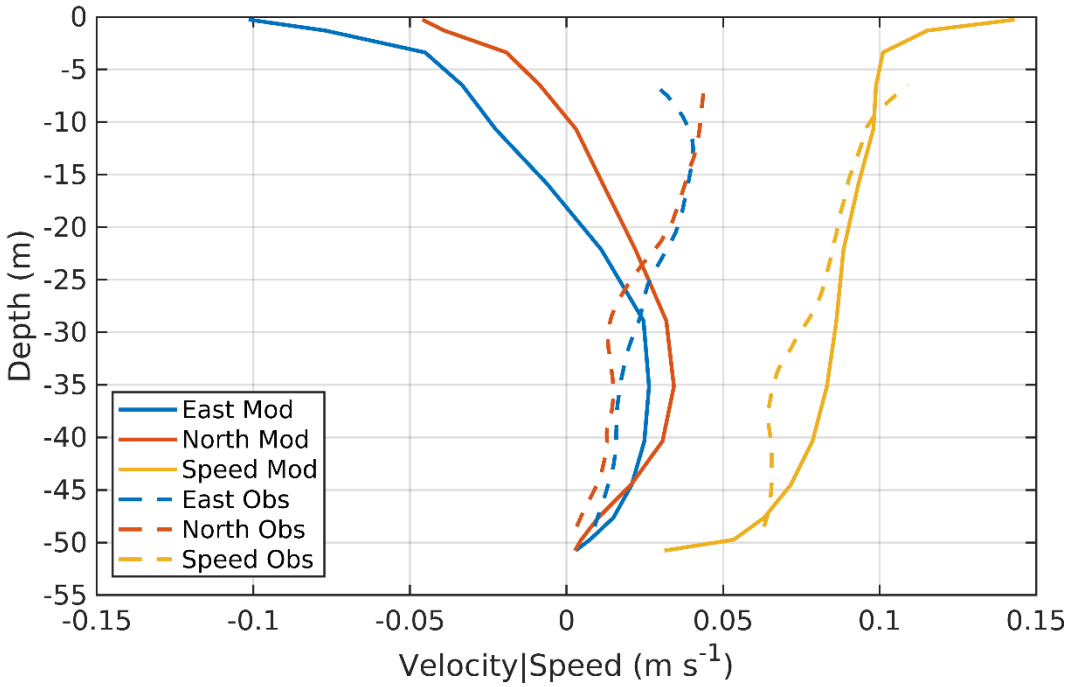


*Figure 15. Profiles of observed and modelled mean velocity (East, North) and mean speed, calculated over the full simulation from April – July 2023.*

## 4.3 Validation: 7th August – 12th October 2023 (ID421, Etive 4)

At the ADCP location, the modelled sea surface height again exhibited a larger tidal range than observed within Loch Etive. The model skill was 0.84 (Figure 16, Table 4), and the mean absolute error (MAE) and root-mean-square error (RMSE) values were 0.38 m and 0.45 respectively.

For the East and North components of near-surface (5.7 m) velocity (Figure 6), the model skill scores were 0.69 and 0.70 respectively, with RMSE values of 0.07 m $s^{-1}$ and 0.15 m $s^{-1}$ for the two components of velocity respectively (Table 2). At the deeper depth of 15.7 m, the skill scores were slightly lower, at 0.65 and 0.68 respectively. The MAE and RMSE values were less than those at the shallower depth, in the range 0.04 m $s^{-1}$ – 0.07 m $s^{-1}$. At the deeper depth (41.7 m), model performance was comparable to the middle depth (Table 2).

The scatter plots and histograms shown in Figure 18 and Figure 19 demonstrate that the modelled currents were broadly of the same speed and direction as the observed data. The vertical profiles of mean velocity and speed (Figure 20) again illustrate the rapid changes in velocity in the top 15 m of the water column, illustrating the challenges in getting good model-data agreement at a fixed depth. The model broadly reproduces the vertical structure of the observed mean flow, although the modelled mean current is weaker in the lower water column than observed.

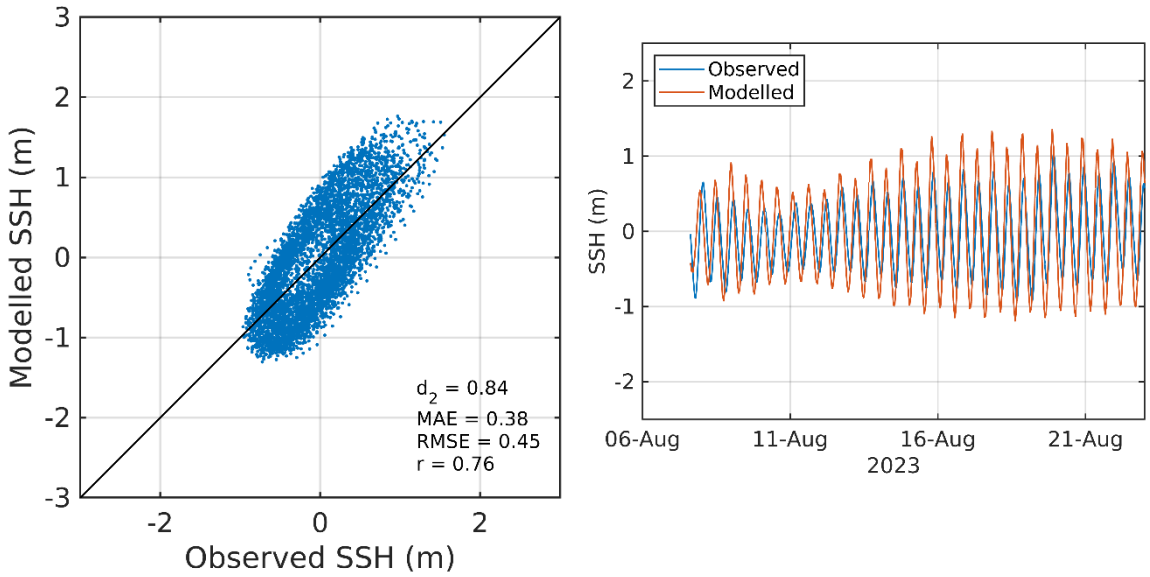


*Figure 16. Comparison between observed and modelled sea surface height from August – September 2018 (ADCP deployment ID421) using model parameter values from Table 1. Both the full record (left) and a subset of 15 days (right) are shown. Observed data are in blue, model results in red*.

*Table 4. Model performance statistics for sea surface height (SSH), and East and North velocity at the Etive 4 ADCP location from the calibration simulation, July – September 2023 (ID421) at two depths, 8.9m and 15.9m.*

| | | Skill, $d_2$ | MAE | RMSE |
|---|---|---|---|---|
| Sea Surface Height (SSH, m) | | 0.84 | 0.38 | 0.45 |
| 5.7 m | East Velocity (m $s^{-1}$) | 0.69 | 0.05 | 0.07 |
| | North Velocity (m $s^{-1}$) | 0.70 | 0.12 | 0.15 |
| 15.7 m | East Velocity (m $s^{-1}$) | 0.65 | 0.04 | 0.05 |
| | North Velocity (m $s^{-1}$) | 0.68 | 0.05 | 0.07 |
| 41.7 m | East Velocity (m $s^{-1}$) | 0.69 | 0.04 | 0.05 |
| | North Velocity (m $s^{-1}$) | 0.65 | 0.04 | 0.05 |

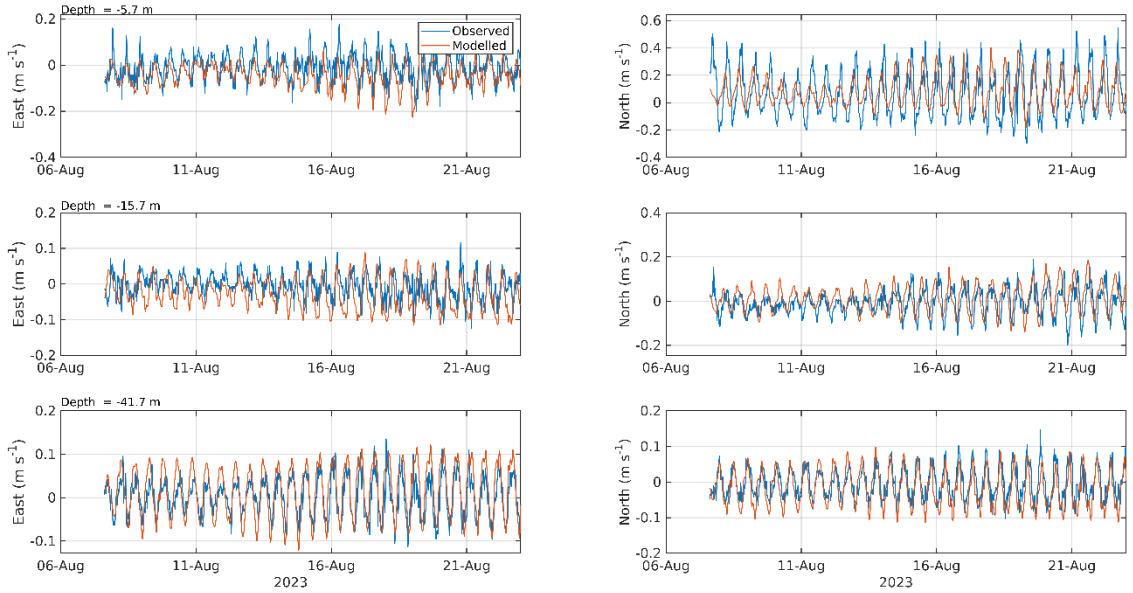


*Figure 17. Comparison between observed and modelled East (left) and North (right) components of velocity at the ADCP location for 15 days in August 2023 (ID421) at three depths, 5.7 m (top), 15.7 m (middle) and 41.7 m (bottom). Observed data are in blue, model results in red.*

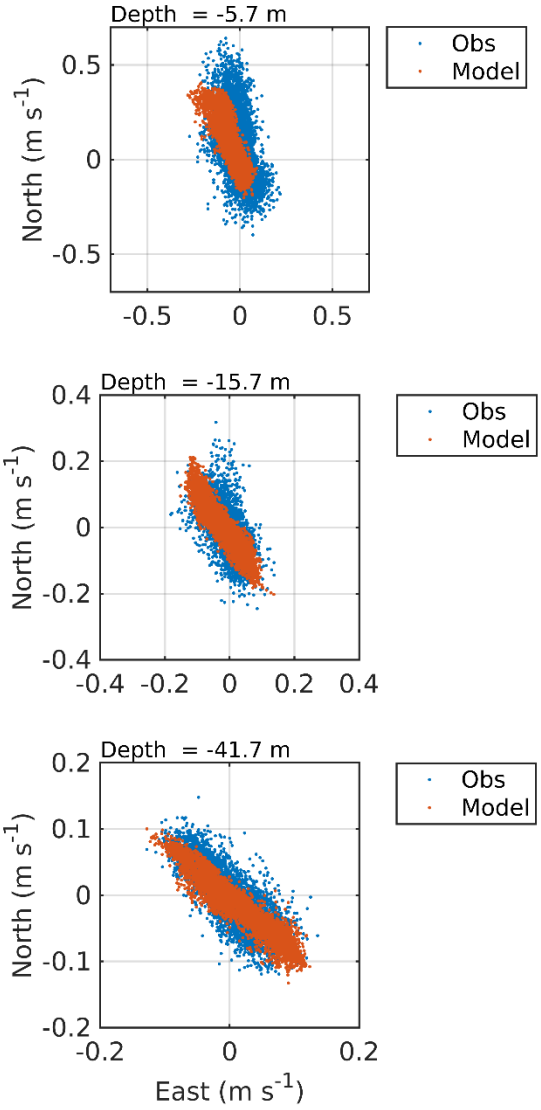


*Figure 18. Scatter plot of observed and modelled velocity at the ADCP location for August – October 2023 (ID421) at three depths, 5.7 m (top), 15.7 m (middle) and 41.7 m (bottom). Observed data are in blue, model results in red.*

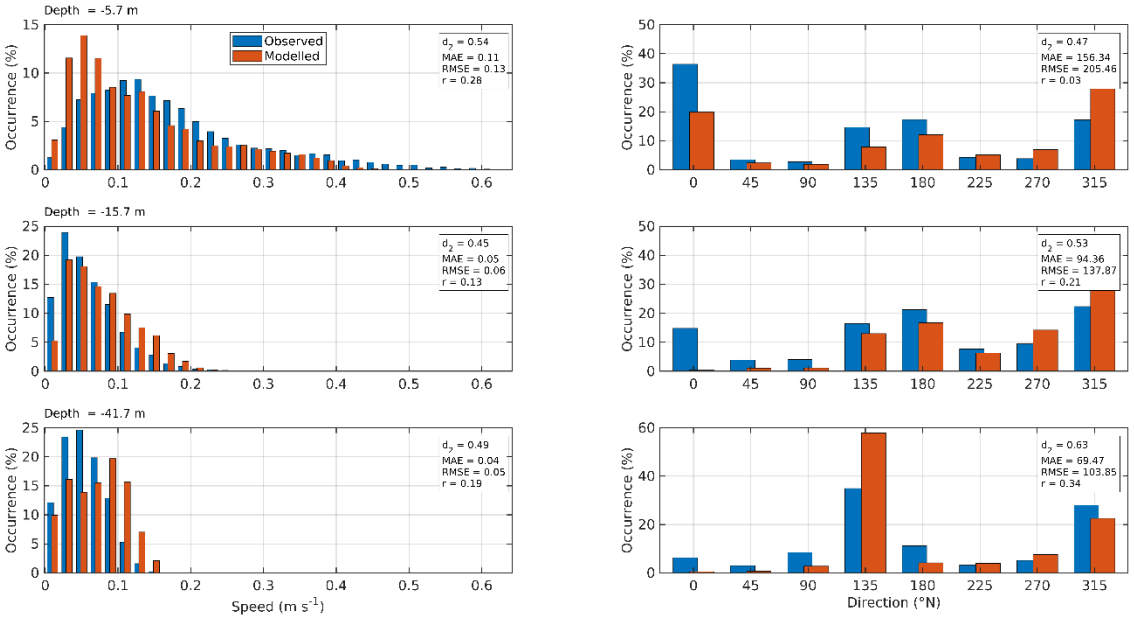


*Figure 19. Histograms of observed and modelled current speed (left) and direction (right) at the ADCP location for August – October 2023 (ID421) at three depths, 5.7 m (top), 15.7 m (middle) and 41.7 m (bottom). Observed data are in blue, model results in red.*

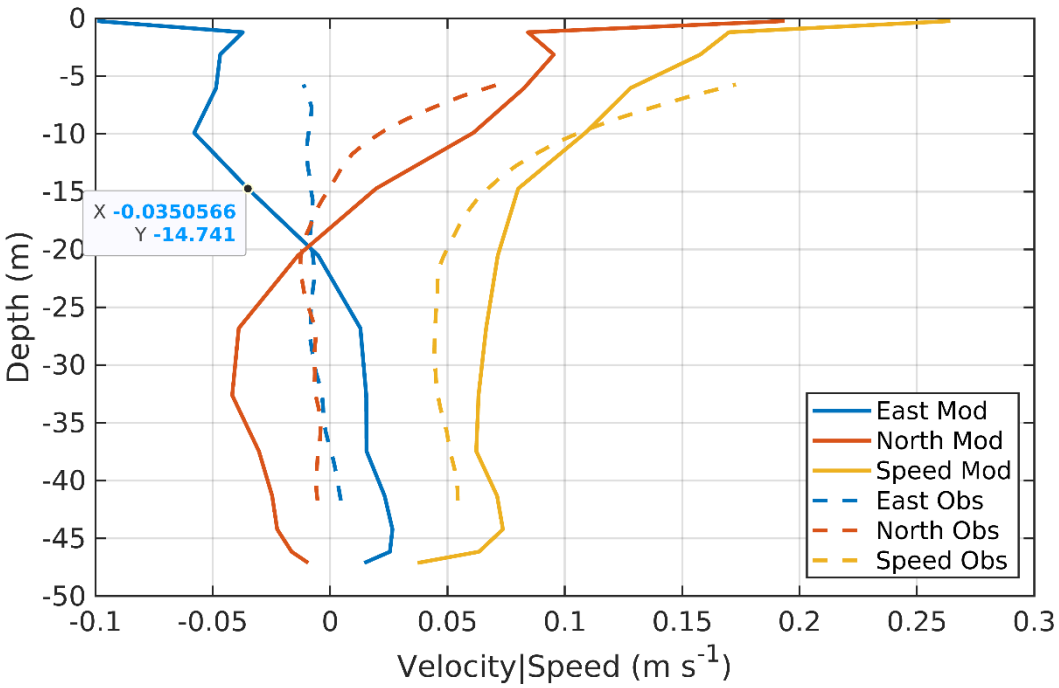


*Figure 20. Profiles of observed and modelled mean velocity (East, North) and mean speed, calculated over the full simulation from 7th August – 12th October 2023.*

# 5. Modelled Flow Fields

Modelled flood and ebb velocity vectors at spring tides are illustrated in Figure 21. Modelled velocity fields from layer 3 in the model (σ = 0.065, midway between sigma-levels 3 and 4) were used in Figure 21 and Figure 22. At the Etive 4 and Etive 6 sites, where water depths were about 45 – 50 m, the depth of the plotted velocity vectors was therefore about 3 m; clearly the depth of the plotted vectors varies spatially as the water depths in the loch vary.

Modelled near-surface current speeds in Loch Etive at springs reached speeds of 0.5 m $s^{-1}$, being markedly stronger on the ebb tide than on the flood, as expected in a stratified sea loch. Modelled currents speeds were weaker during neap tides.

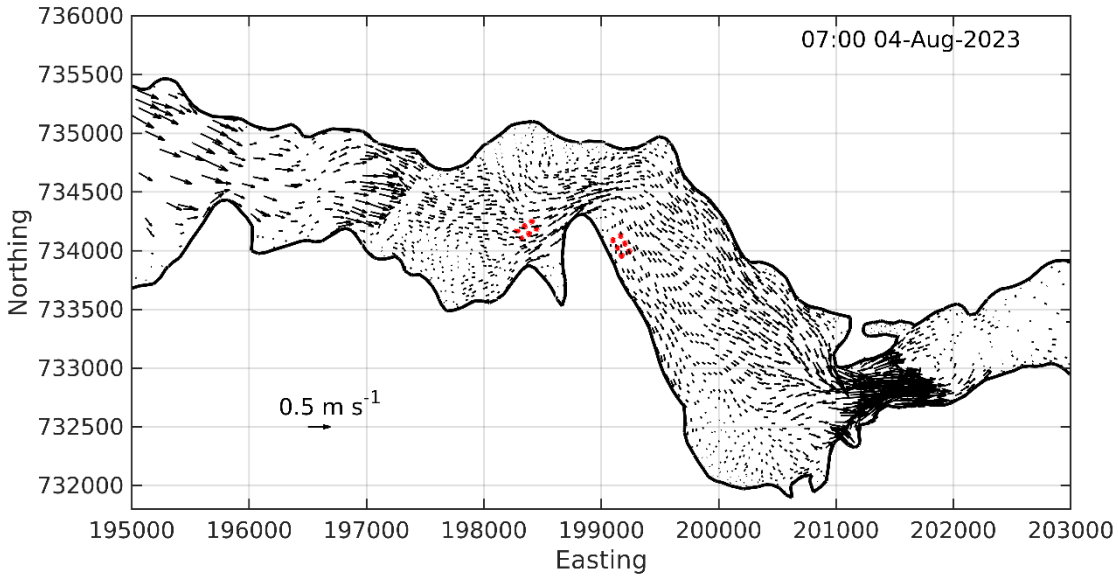


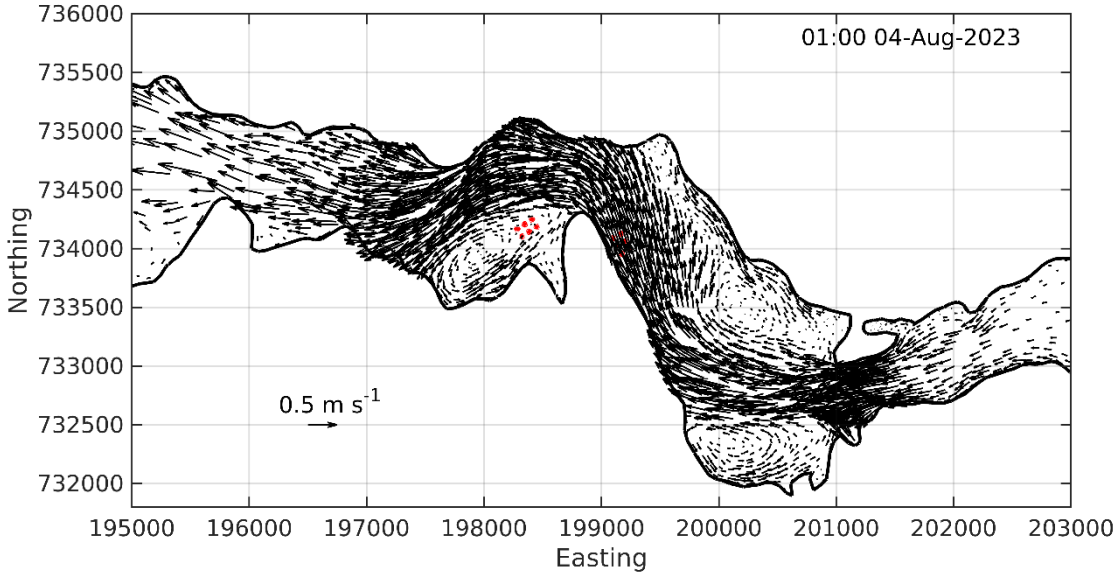

*Figure 21. Modelled flood (top) and ebb (bottom) near-surface current vectors during spring tides at 07:00 and 01:00 on 4th August 2023 respectively. For clarity, only 20% of the model vectors are shown.*

The mean (residual) near-surface currents are seaward within Loch Etive (Figure 22), again as expected in a stratified sea loch. The model indicates the presence of several residual gyres within the nearshore bays of the sea loch, between which the prevailing flow threads a route to sea. However, these residual flows indicate that patches of medicine following treatment at the Etive 4 and Etive 6 sites will be transported quite rapidly westward to the entrance of Loch Etive and into Ardmucknish Bay, where dispersion and dilution is likely to be rapid.

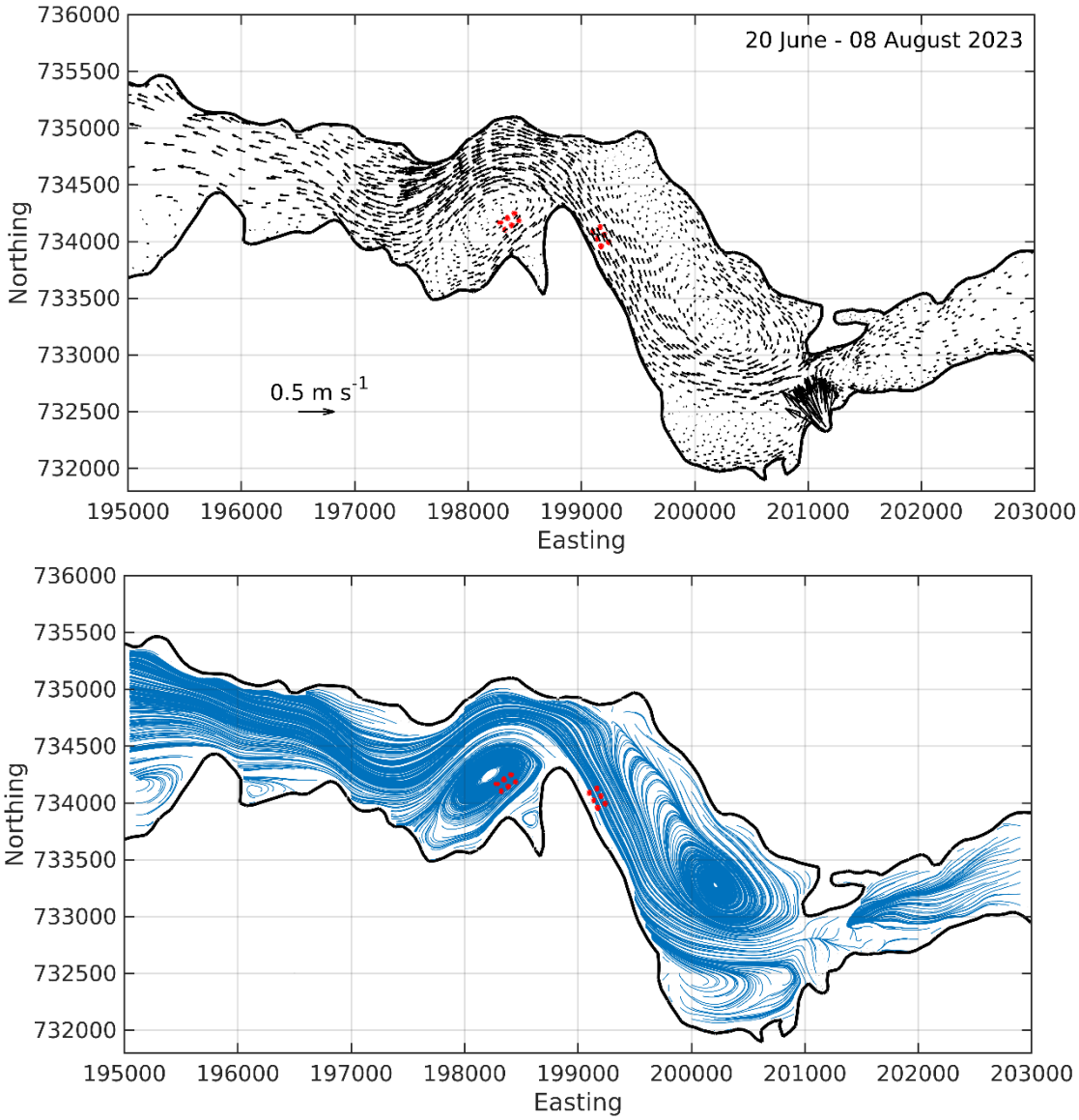


*Figure 22. Modelled mean (residual) near-surface current vectors (top) and streamlines (bottom) averaged over the full simulation from 20th June – 8th August 2023. For clarity, only 20% of the model vectors are shown.*

## 6. Conclusions

This report demonstrates that the hydrodynamic model reproduces the measured currents in Loch Etive acceptably well given the challenges of modelling this enclosed, highly stratified and dynamic environment. The magnitude and direction of the modelled currents at all depths is broadly correct. In addition, the near-surface residual flows, which will determine the net transport of discharges, are reasonably well simulated. We conclude that the model is suitable for simulating the transport and dispersion of bath medicines from the Etive 4 and Etive 6 salmon farm sites.

## 7. References

Aleynik, D. Davidson, K., Dale A. C. and Porter, M., 2016. A high resolution hydrodynamic model system suitable for novel harmful algal bloom modelling in areas of complex coastline and topography. Harmful Algae, 53(3):102–117, 10.1016/j.hal.2015.11.012

Burchard, H., 2002. Applied turbulence modeling in marine waters. Springer:Berlin-Heidelberg-New York-Barcelona-Hong Kong-London-Milan Paris-Tokyo, 215pp.

Chen, C., H. Liu, and R.C. Beardsley, 2003. An unstructured, finite-volume, three-dimensional, primitive equation ocean model: Application to coastal ocean and estuaries. J. Atmos. Ocean. Tech., 20, 159 – 186.

Edwards, A. and Sharples, F., 1986. Scottish Sea Lochs: A Catalogue. Scottish Marine Biological Association, Dunstaffnage Marine Laboratory, Oban, U.K., 400pp.

ECMWF, 2021. ERA5 Dataset, European Centre for Medium-Range Weather Forecasts. Available at https://www.ecmwf.int/en/forecasts/datasets/reanalysis-datasets/era5

Gillibrand, P.A., Walters, R.A., and McIlvenny, J., 2016. Numerical simulations of the effects of a tidal turbine array on near-bed velocity and local bed shear stress. *Energies*, vol 9, no. 10, pp. 852. DOI: 10.3390/en9100852

Large. W.G. and Pond, S., 1981. Open ocean momentum flux measurements in moderate to strong winds. J. Phys. Oceanogr., 11, 324—336.

Marine Scotland, 2016. Scottish Shelf Model. Part 4: East Coast of Lewis and Harris Sub-Domain. Available at https://www.gov.scot/publications/scottish-shelf-model-part-4-east-coast-lewis-harris-sub/pages/4/

Mowi, 2024. Hydrodynamic and Bath Medicine Dispersion Modelling at Aird Point (Etive 4) and Sailean Ruadh (Etive 6) sites.

Pawlowicz, R., Beardsley, R., Lentz, S., 2002. Classical tidal harmonic analysis including error estimates in MATLAB using T_TIDE. Computers and Geosciences, 28, 929-937.

Umlauf, L.; Burchard, H. 2003. A generic length-scale equation for geophysical turbulence models, J. Mar. Res., 61, 235-265.

Walters, R.A.; Casulli, V., 1998. A robust, finite element model for hydrostatic surface water flows. Comm. Num. Methods Eng., 14, 931–940.

Warner, J.C.; Sherwood, C.R.; Arango, H.G.; Signell, R.P.; 2005. Performance of four turbulence closure models implemented using a generic length scale method. Ocean Modelling, 8, 81 – 113.

Willmott, C. J.; Ackleson, S. G.; Davis, R. E.; Feddema, J. J.; Klink, K. M.; Legates, D. R. O'Donnell, J.; Rowe, C. M. 1985. Statistics for evaluation and comparison of models, J. Geophys. Res., 90, 8995– 9005.